8 March 2010 Elazığ-Kovancılar (Turkey) Earthquake: Observations on Ground Motions and Building Damage

Sinan Akkar,[1] Alper Aldemir,[1] Aysegul Askan,[1, 2] Sadık Bakır,[1] Erdem Canbay,[1] İ. Ozan Demirel,[1] M. Altug Erberik,[1] Zeynep Gülerce,[1] Polat Gülkan,[1] Erol Kalkan,[3] Surya Prakash,[4] M. Abdullah Sandıkkaya,[1] Volkan Sevilgen,[3] Beliz Ugurhan,[1] and Emrah Yenier[1]

INTRODUCTION

An earthquake of $M_W = 6.1$ occurred in the Elazığ region of eastern Turkey on 8 March 2010 at 02:32:34 UTC. The United States Geological Survey (USGS) reported the epicenter of the earthquake as 38.873°N-39.981°E with a focal depth of 12 km. Forty-two people lost their lives and 137 were injured during the event. The earthquake was reported to be on the left-lateral strike-slip east Anatolian fault (EAF), which is one of the two major active fault systems in Turkey. Teams from the Earthquake Engineering Research Center of the Middle East Technical University (EERC-METU) visited the earthquake area in the aftermath of the mainshock. Their reconnaissance observations were combined with interpretations of recorded ground motions for completeness. This article summarizes observations on building and ground damage in the area and provides a discussion of the recorded motions. No significant observations in terms of geotechnical engineering were made.

SEISMOTECTONICS OF THE REGION

The major tectonic structure in Turkey is the north Anatolian fault zone (NAFZ), with right-lateral faulting extending from Istanbul in the west to Karlıova in the east. During the twentieth century this fault zone has produced several large earthquakes ($M_S > 7$) with surface rupturing with a westward migrating sequence as demonstrated in Figure 1 (Barka 1996; Utkucu *et al.* 2003). Around the Karlıova region, NAFZ joins the southwest-trending east Anatolian fault zone (EAFZ). The EAFZ is predominantly left-lateral strike-slip in nature, but its faulting is less continuous and less localized than that of the NAFZ (Ambraseys 2009). The EAFZ has nucleated relatively small magnitude earthquakes in the twentieth century (Figure 1).

Recent GPS data indicates that the slip rate in the EAFZ has an upper bound of 8±1 mm/year (Ambraseys 2009). The epicenter (by USGS) of the 8 March 2010 Elazığ-Kovancılar earthquake is in the segmented fault region of the EAFZ to the south of the Karakoçan region with a left-lateral strike-slip faulting mechanism. However, no surface rupturing was observed in the field. Figure 1 shows the active faults in the region and the strong-motion stations that recorded the mainshock.

POSTULATED STRESS TRANSFER

Rupture orientation of the 2010 Elazığ-Kovancılar earthquake was inferred from the aftershock distribution and the USGS body wave focal mechanism, which is left-lateral strike-slip fault with 47° strike, 75° dip, and −4° rake angles. In the Coulomb stress calculation, a 10 by 7 km rupture area with a 0.5 m uniform slip is assumed as the Coulomb source fault based on the Wells and Coppersmith (1994) relationship. A static Coulomb stress transfer model was computed for the Kovancılar earthquake to promote failure by 0.1 bar on the east Anatolian fault as shown in Figure 2. That level of stress increase may induce seismicity on the adjacent active faults (Lin and Stein 2004; Toda *et al.* 2005).

RECORDED GROUND MOTIONS AND GROUND-MOTION PREDICTIONS

Ground motions recorded at the stations shown in Figure 1 are plotted in terms of three-component acceleration time histories in Figure 3. Peak ground accelerations and spectral accelerations computed at $T = 0.2$ s and $T = 1$ s are then compared with predictions. Several ground motion prediction equations (GMPEs) are used to characterize ground-motion variation with distance. Recorded raw acceleration time series were first corrected by trend removal including pre-event mean, and

1. Earthquake Engineering Research Center, Middle East Technical University, Ankara, Turkey
2. Corresponding author
3. U.S. Geological Survey, Menlo Park, California, U.S.A.
4. National Institute of Disaster Management, New Delhi, India

doi: 10.1785/gssrl.82.1.42

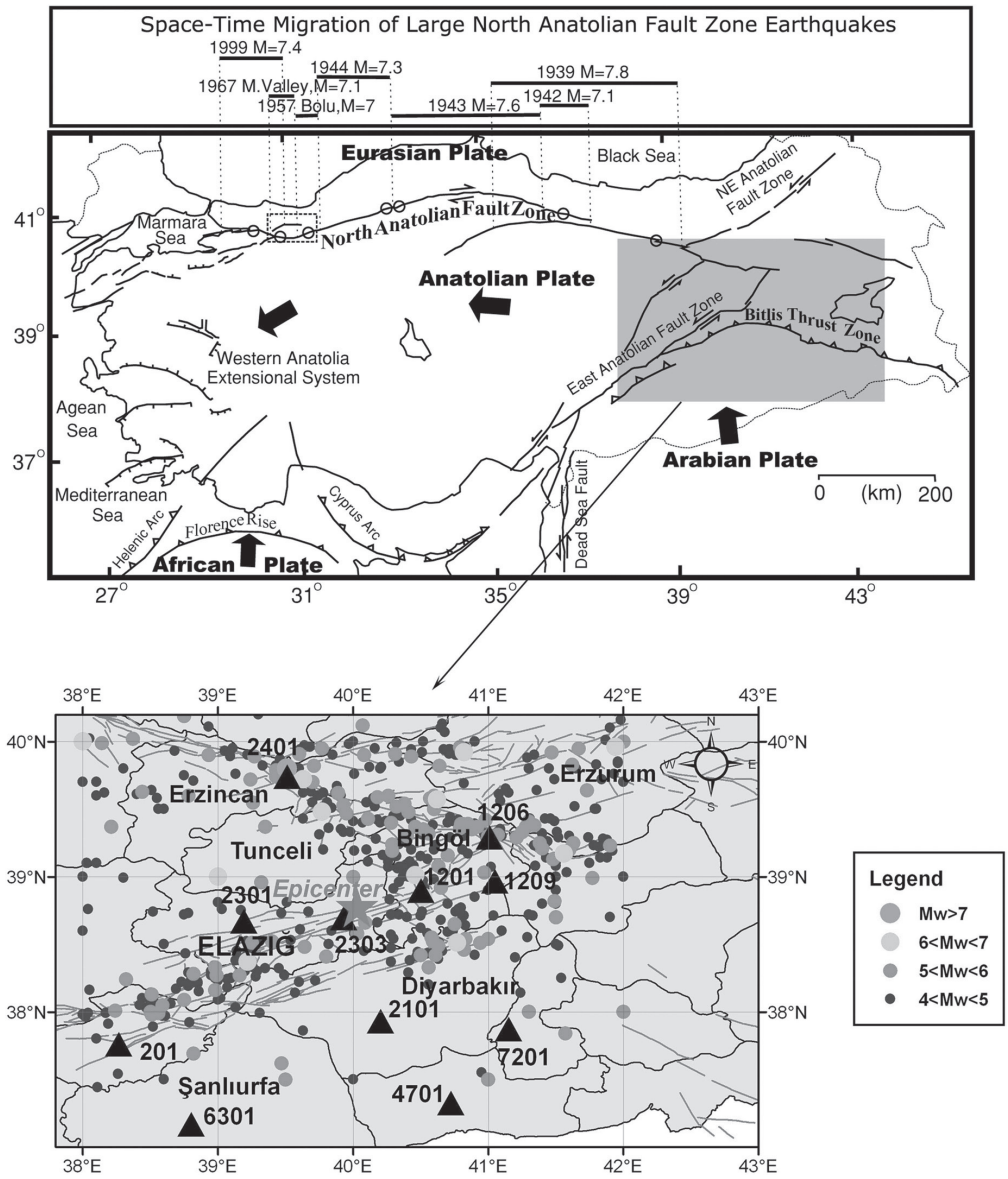

▲ **Figure 1.** Tectonic structure of Turkey (top) and seismicity of the EAFZ during the last century (bottom). Top figure is adapted from Barka 1996 and Utkucu *et al.* 2003. The star indicates the epicenter of the Elazığ-Kovancılar earthquake and the black triangles indicate strong-motion stations operated by the Disaster and Emergency Management Authority of Turkey (DEMA). Active faults in the region are adapted from the active fault map of Saroglu *et al.* (1992).

then uniformly filtered by fifth-pole acasual Butterworth filter with cut-off frequencies of 0.2 Hz and 20 Hz, respectively. Although the choice of high- and low-pass filter cut-offs is generally based on the frequency content of each record, the processing applied is adequate for the model comparisons presented in this article. Baseline correction based on a segmental polynomial was applied to ensure that displacement and velocity converge to zero at the termination of each record (Kalkan and Kunnath 2006; Boore *et al.* 2002; Graizer 1989). Using the corrected records, we computed 5% damped response spectral ordinates for each component of ground motion. Table 1 shows peak-ground acceleration (PGA) and spectral accelerations (SA) at 0.2 s and 1 s for eleven records. Also listed are the characteristics of stations and distance metrics. The closest station was at 17 km to the epicenter, while the remaining ones were at moderate to long distances away. Selected GMPEs utilize two unique definitions of distance parameter specific to the model. In the first case, the distance measure is the Joyner-Boore distance definition (R_{JB}), defined as the closest distance from the recording station to the surface projection of the fault rupture plane (Boore *et al.* 1997). In the second case, the distance measure is the "closest fault distance" (R_{CL}), defined as the closest distance to the co-seismic rupture plane (Campbell and Bozorgnia 2008). GMPEs selected are those of Kalkan and Gülkan (2004) [KG04], Boore and Atkinson (2008) [BA08], and Akkar and Cagnan (2010) [AC10] utilizing R_{JB} definition; and Graizer and Kalkan (2007, 2009) [GK07], Campbell and Bozorgnia (2008) [CB08], and Chiou and Youngs (2008)

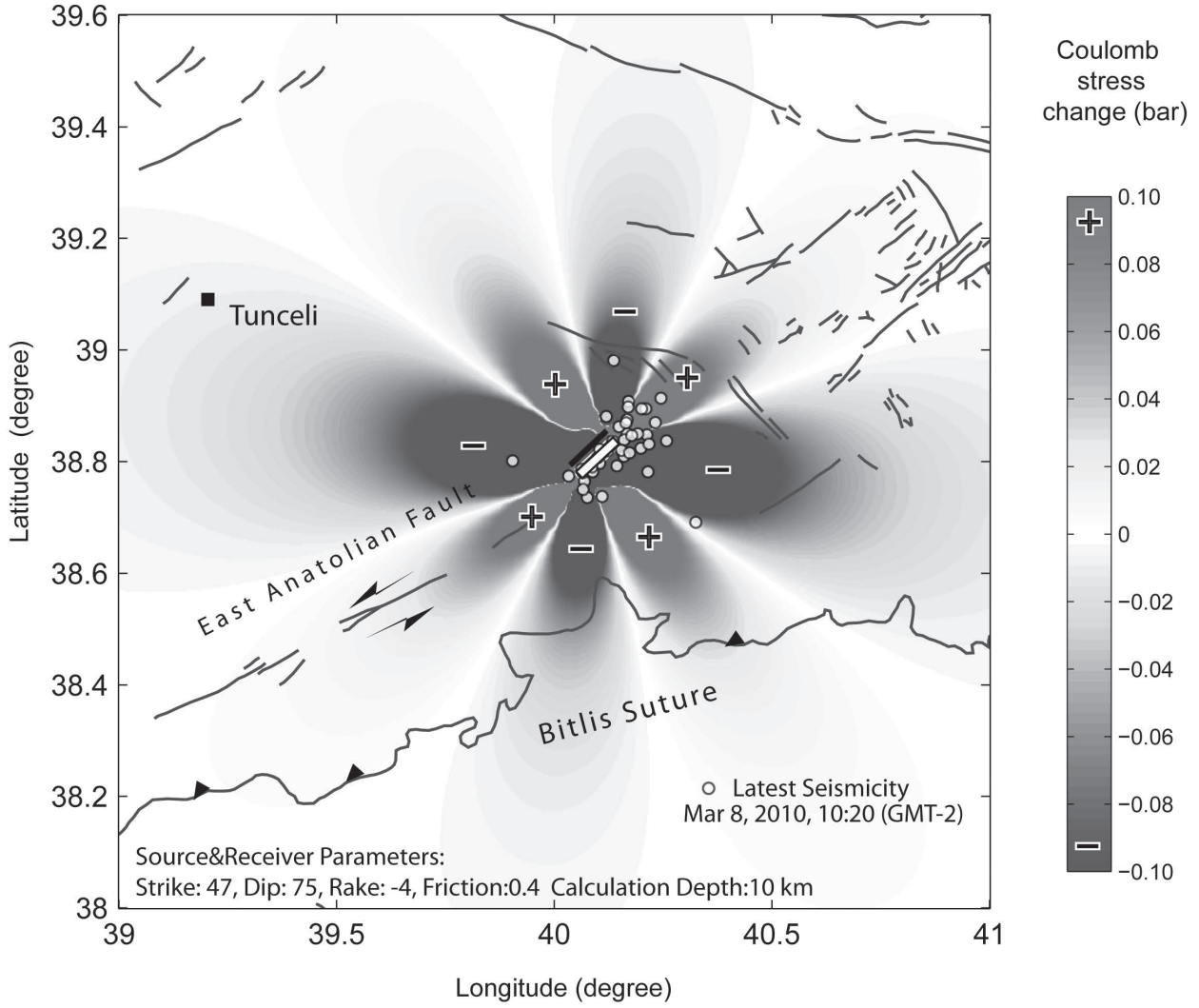

▲ **Figure 2.** Elazığ-Kovancılar earthquake increased the static Coulomb stress on the east Anatolian fault. Rectangle is the Coulomb source fault. Black circles are the aftershocks.

TABLE 1
Selected ground motion records and details of stations (source: http://daphne.deprem.gov.tr:89/2K/daphne_v4.php).

Station Information								Distance Measure	Peak Values (EW) (cm/s^2)		Peak Values (NS) (cm/s^2)		
City	Province	Station Code	Latitude	Longitude	V_{S30} (m/s)	R_{CL} (km)	R_{JB} (km)	PGA	SA(0.2s)	SA(1.0s)	PGA	SA(0.2s)	SA(1.0s)
Adıyaman	Merkez	201	37.7612	38.2674	391	192.4	191.6	2.3	2.6	2.9	2.5	2.9	4.0
Bingöl	Merkez	1201	38.8971	40.5032	529	40.5	36.8	33.9	89.2	41.5	53.8	89.3	46.6
Bingöl	Karlıova	1206	39.2935	41.0088	356	91.8	90.3	17.6	40.8	24.8	11.6	45.9	16.8
Bingöl	Solhan	1209	38.9660	41.0499	463	87.0	85.4	28.9	64.3	16.8	28.9	59.4	11.2
Diyarbakır	Merkez	2101	37.9309	40.2028	519	105.3	103.9	5.0	11.4	4.4	3.3	12.4	4.2
Elazığ	Merkez	2301	38.6704	39.1927	407	72.4	70.1	4.5	12.1	4.4	5.5	13.2	4.7
Elazığ	Palu	2303	38.6958	39.9319	329	24.2	17.3	66.2	94.8	52.9	61.7	116.1	71.4
Mardin	Merkez	4701	37.3263	40.7237	709	182.2	181.4	2.5	2.8	1.5	2.6	2.6	1.1
Urfa	Merkez	6301	37.1681	38.8014	N/A	209.0	208.3	1.4	2.6	1.3	1.6	2.9	1.9
Batman	Merkez	7201	37.8730	41.1511	450	150.3	149.3	5.4	7.6	1.3	7.6	7.5	1.0
Erzincan	Merkez	2401	39.7418	39.5115	314	104.0	102.1	6.9	18.3	17.1	8.9	30.4	10.9

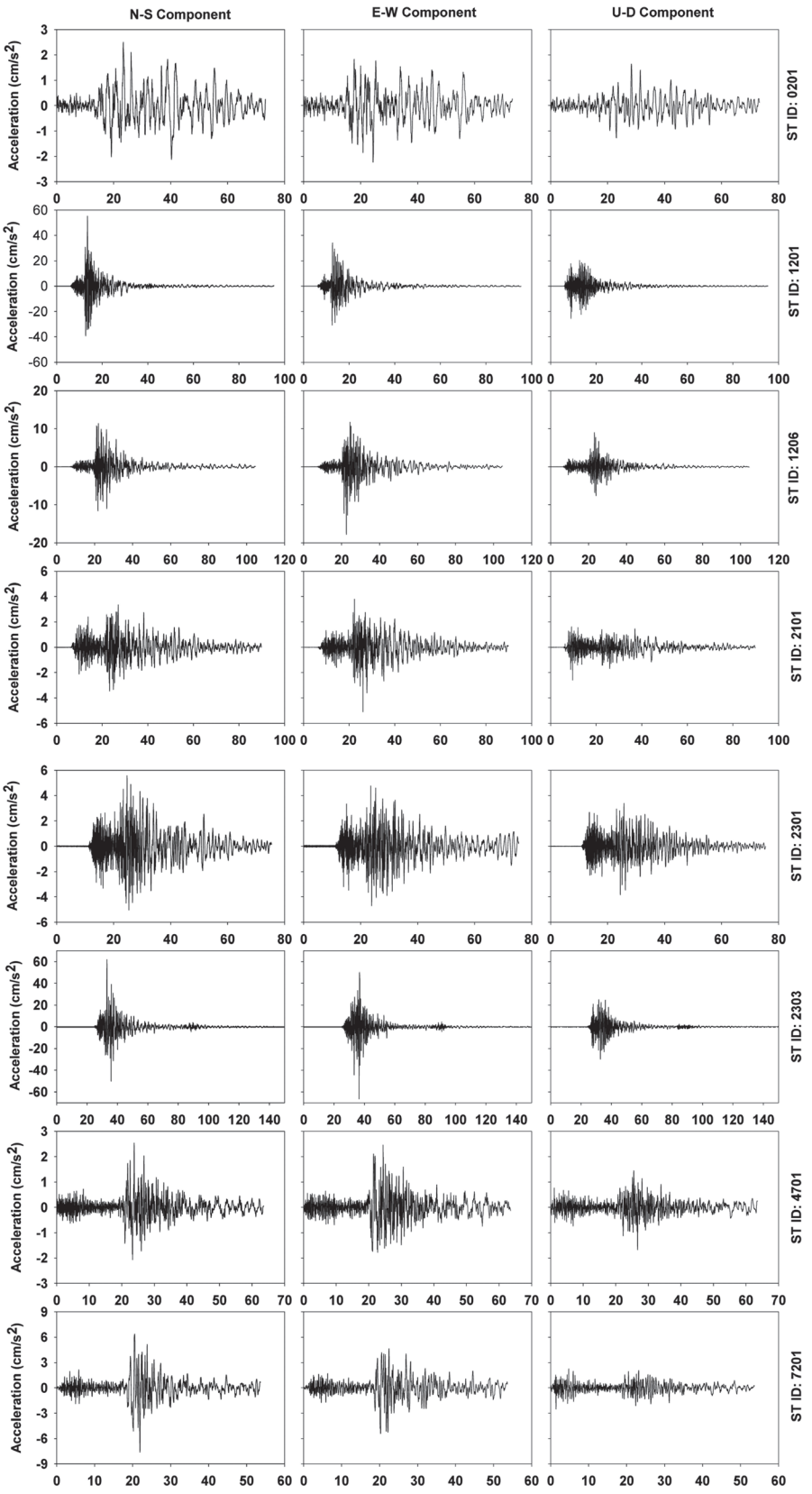

▲ **Figure 3.** Acceleration time series of the processed ground motions recorded from the 8 March 2010 02:32:29 Elazığ-Kovancılar, earthquake. North-south (NS), east-west (EW), and up-down (UD) components are plotted left, middle, and right columns, respectively.

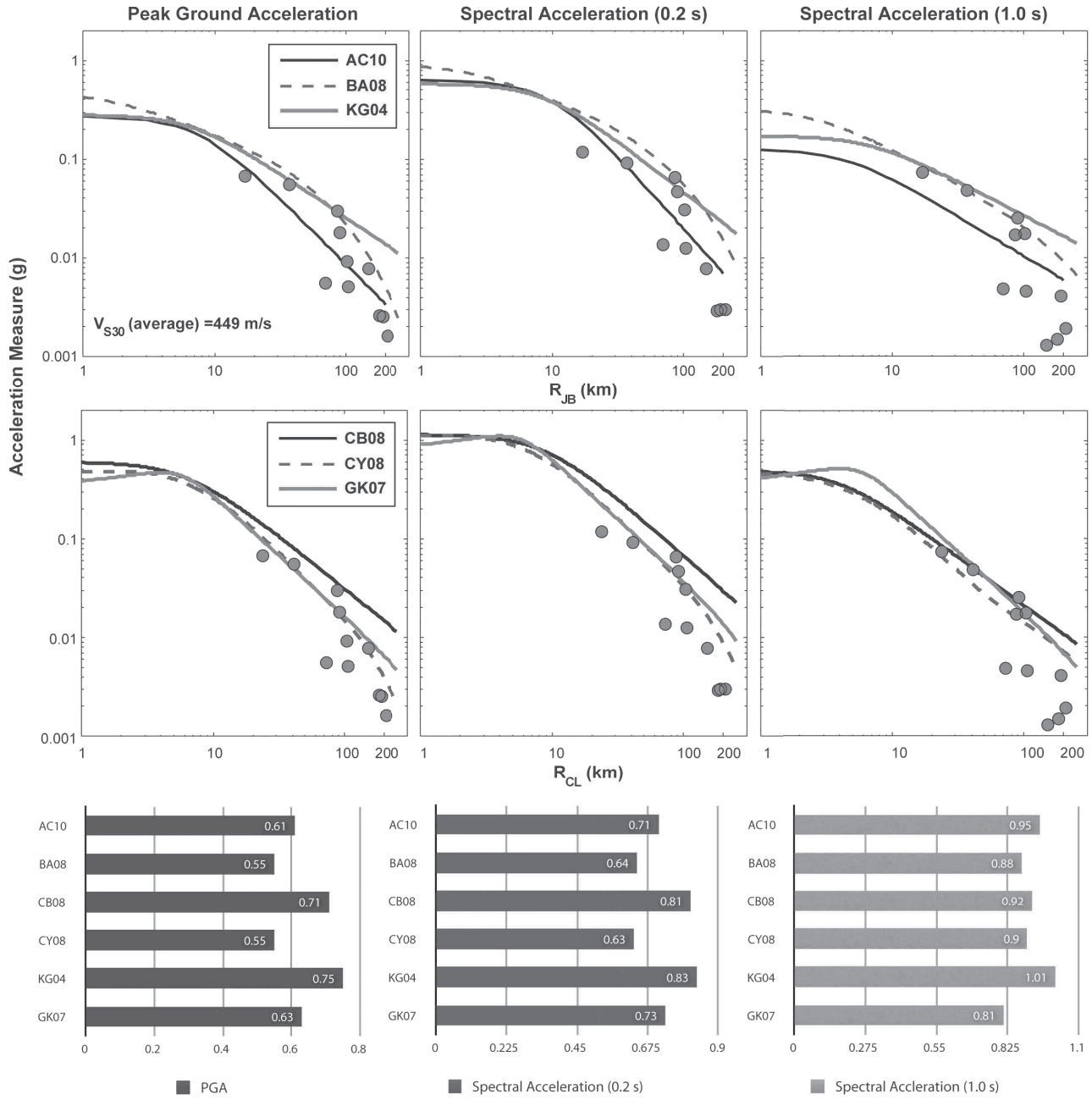

▲ **Figure 4.** A) Comparison of PGA, SA at T = 0.2 s, and SA at T = 1.0 s values recorded from the mainshock (**M** 6.0 on strike-slip fault at 5 km depth) with six different GMPEs considering two distance measures. Top panels: Predictions considering R_{JB} for AC10—Akkar and Cagnan 2010; BA08—Boore and Atkinson 2008; KG04—Kalkan and Gülkan 2004; [Bottom panels] Predictions considering R_{CL} for CB08—Campbell and Bozorgnia 2008; CY08—Chiou and Youngs 2008; GK07—Graizer and Kalkan (2007, 2009). Ground-motion data shows faster attenuation at far distances due to apparent regional low *Q* (Zor *et al.* 2007). B) Standard error (σ_{lnY}) of predictions computed for each GMPE for PGA, SA (0.2 s), and SA (1.0 s) using maximum horizontal components from eleven ground motion records. The average standard error of six GMPEs is 0.63, 0.73, and 0.91 respectively for PGA, SA at 0.2 s and SA at 1.0 s.

[CY08] that use "closest fault distance." Among these, the KG04 and AC10 are based on indigenous datasets compiled from Turkish earthquakes. The GK07, BA08, CB08, and CY08 are based on the PEER-NGA database (Chiou *et al.* 2008), which also contains earthquake records from Turkey.

Figure 4A compares the PGA, SA at 0.2 s, and SA at 1 s with six GMPEs based on the two different distance measures. The attenuation curves are plotted for the average V_{S30} of eleven stations ($V_{S30,ave} = 450$ m/s), which corresponds to NEHRP site class site class C (Sandıkkaya *et al.* 2010). Maximum values from two horizontal components of each record are utilized (shown by filled circles). Because the AC10, BA08, CB08 and CY08 predict geometric mean of ground motion, their predictions are adjusted for themaximum horizontal component

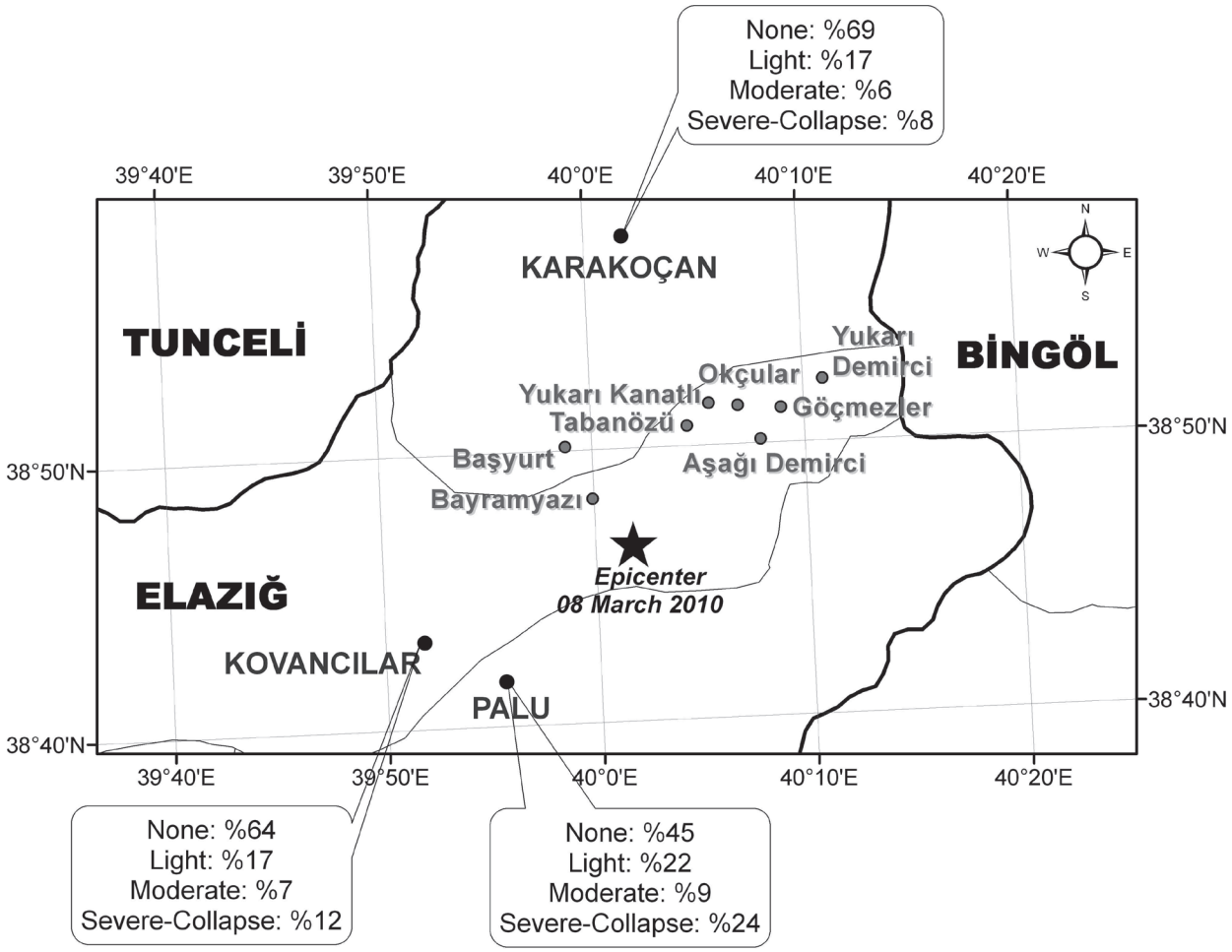

▲ **Figure 5.** The villages that had severe structural damage during the 8 March 2010 Kovancılar earthquake and the percentage of damage states of residential units in the county-size districts of Kovancılar, Karakoçan, and Palu.

by multiplying their predictions with 1.11, 1.11, and 1.118 for PGA, SA at 0.2 s and SA at 1 s, respectively. These adjustment factors were adapted from Campbell and Bozorgnia (2008). The other GMPEs (KG04 and GK07) predict the maximum of the two horizontal components.

As seen in Figure 4A, the GMPEs indicate an overall good fit to recorded data up to about 100 km from the fault for PGA, SA at 0.2 s, and SA at 1 s. Beyond 100 km, there is notable overestimation. Actual data show faster attenuation with the order R^{-4} beyond 100 km and slower attenuation with the order $R^{-1.5}$ at closer distances to the fault. Faster attenuation of ground motion is due to the low Q of the crustal structure in this particular region of eastern Turkey (Zor *et al.* 2007). For PGA, faster attenuation of PGA (R > 100 km) is reasonably captured by AC10, BA08, CY08, and GK07; the CB08 and KG04 overpredict the actual data beyond 100 km. For SA at 0.2 s at R > 100 km, AC10, CY08, and GK07 are the only three models that provide the good predictions. For SA at 1 s, predictions of BA08, CB08, CY08, and GK07 within 20 to 100 km are similar to each other and fit reasonably well to actual data. Particularly for SA at 1 s, predictions of AC10 at all distances are much lower than those of the other five models. For half of the data points, all GMPEs overpredict the SA at 1 s, particularly the data beyond 100 km; the overprediction is more significant for KG04. To quantify the quality of fit, the standard error (σ_{InY}) of prediction for each GMPE is computed based on residuals corresponding to eleven data points; in computing σ_{InY}, the exact value of V_{S30} for each station is utilized. The comparisons of standard error are demonstrated in Figure 4B for PGA, SA at 0.2 s, and SA at 1 s. We note that although the prediction curves were plotted based on the average V_{S30} of eleven stations, the standard error of each GMPE was computed based on the exact V_{S30} of each station.

EFFECTS OF THE EARTHQUAKE ON BUILDINGS

The earthquake caused major structural damage and fatalities in only a few villages (Okçular, Göçmezler, Yukarı Kanatlı, Yukarı Demirci, and Tabanözü), shown in Figure 5. Nearby towns and provinces were not seriously affected. The main reason for widespread damage in villages close to the epicenter can be explained by considering the building types and construction practices in the affected region. Figure 5 shows the percentage of damage states of residential units in the county-size districts of Kovancılar, Karakoçan and Palu out of a total

of 9,000, 9,000, and 5,000 dwelling units, respectively (source: http://www.elazig.gov.tr/).

LOCAL CONSTRUCTION MATERIALS

Dictated by the climate of the region, adobe, stone, and hollow factory brick are the most commonly used construction materials. Adobe is produced from local clayey soil mixed with straw and dried under the sun. Although there are no material tests available, it might be inferred from field observations (adobe is easily broken into small pieces by hand) that adobe units have very low strength with respect to the density of the material. Local stone is used in an irregular fashion without shaping into regular geometry. Hollow factory brick is used as a load-bearing material, although this is not allowed by the regulatory Turkish Earthquake Code (2007). Mud is utilized both as bonding material between brick units and for plastering.

Rural masonry buildings are characterized in two different ways according to the roof material used. The first kind of roof is heavy condensed soil laid over a wooden slab that is in turn supported by wooden logs. The second type is light metal sheets supported by wooden girders and columns (Figure 6).

A significant percentage of the building stock in the affected area is composed of one- or two-story masonry buildings constructed with thick adobe or stone walls, very low-quality mortar, and wooden beams covered by either earthen or sheet metal roofs. It might be appropriate to classify buildings in the affected area into four groups depending on their structural characteristics (Table 2). In order to eliminate the country-specific characteristics of building typology in the affected region, we assigned a vulnerability class to each building type according to the European Macroseismic Scale (Grünthal 1998). EMS vulnerability classes range between A and F, with letter A representing the most vulnerable class.

Type I buildings constitute the most vulnerable structural system. Many such buildings have collapsed in past earthquakes resulting in the loss of lives. The thickness of the condensed soil at the roof is between 30 and 50 cm. Such heavy roofs induce large inertial forces during earthquakes, which result in high stresses on low-strength walls. Roof cave-in becomes a death trap for the people inside the building (Figure 7A). We assign EMS vulnerability class A to this type of building.

Type II buildings are more resistant to earthquake effects than Type I buildings due to their lighter roofs, properly placed horizontal bond beams, relatively better corner connections, and better vertical alignment of openings. This type of building is not earthquake resistant but can withstand earthquakes of moderate intensity since some basic rules of thumb have been considered during construction. Therefore, the buildings in this category experienced some damage during the Elazığ Kovancılar earthquake, but total collapse was usually prevented (Figure 7B). We assign EMS vulnerability class B to this type of building.

Type III buildings are frequently encountered and are the most complex structural systemsin Turkish construction practices. Their ground story is often used as a barn or for storage. It is generally made of stone, but there are also cases where adobe is used. The second story is used for residential purposes and is generally made of hollow factory brick. The main problem in this type of building is the incompatibility of the materials used for different stories and their improper connection to each other. Partial out-of- plane collapse of second-story walls is a typical damage pattern for this type of building (Figure 7C). We assign EMS vulnerability class A to this type of building.

Type IV buildings are rarely observed in the field. Reinforced concrete columns, beams, and slabs are the load-bearing members. Unlike Type I, II, and III buildings, rigid diaphragm action is valid for this type of building due to the stiff concrete slab. However, the material quality is poor and construction practice does not generally conform to fundamental requirements of earthquake-resistant design. It should not be surprising that this type of building exhibited an adequate performance with limited damage during such a moderate earthquake (Figure 7D). We assign EMS vulnerability class C to this type of building.

OBSERVED STRUCTURAL DAMAGE

Rural Masonry Buildings (Type I, Type II, and Type III)

The failure modes of rural masonry buildings observed in the field are out-of-plane failure of walls and gable end walls, in-plane failure of walls, total or partial collapse of the buildings due to the absence of structural integrity, and collapse of the roof. We can see from the site observations that out-of-plane failure of walls and gable end walls are a frequent mode of failure. The main causes of this are stability problems that arise from large unsupported wall lengths in the absence of lateral supporting walls (Figure 8A), poor wall-to-floor connections

TABLE 2
Structural Classification of Buildings in the Affected Region

Type I	Non-engineered rural masonry with adobe or stone walls, low-quality mortar, heavy earthen roof. EMS vulnerability class A.
Type II	Non-engineered rural masonry with adobe or stone walls in the presence of lintels and horizontal bond beams, low-quality mortar, light steel metal roof. EMS vulnerability class B.
Type III	Mixed masonry construction with stone walls in the first story and adobe or hollow factory brick walls in the second story, light steel metal roof. EMS vulnerability class A.
Type IV	Substandard reinforced concrete frame buildings with poor material and construction quality. EMS vulnerability class C.

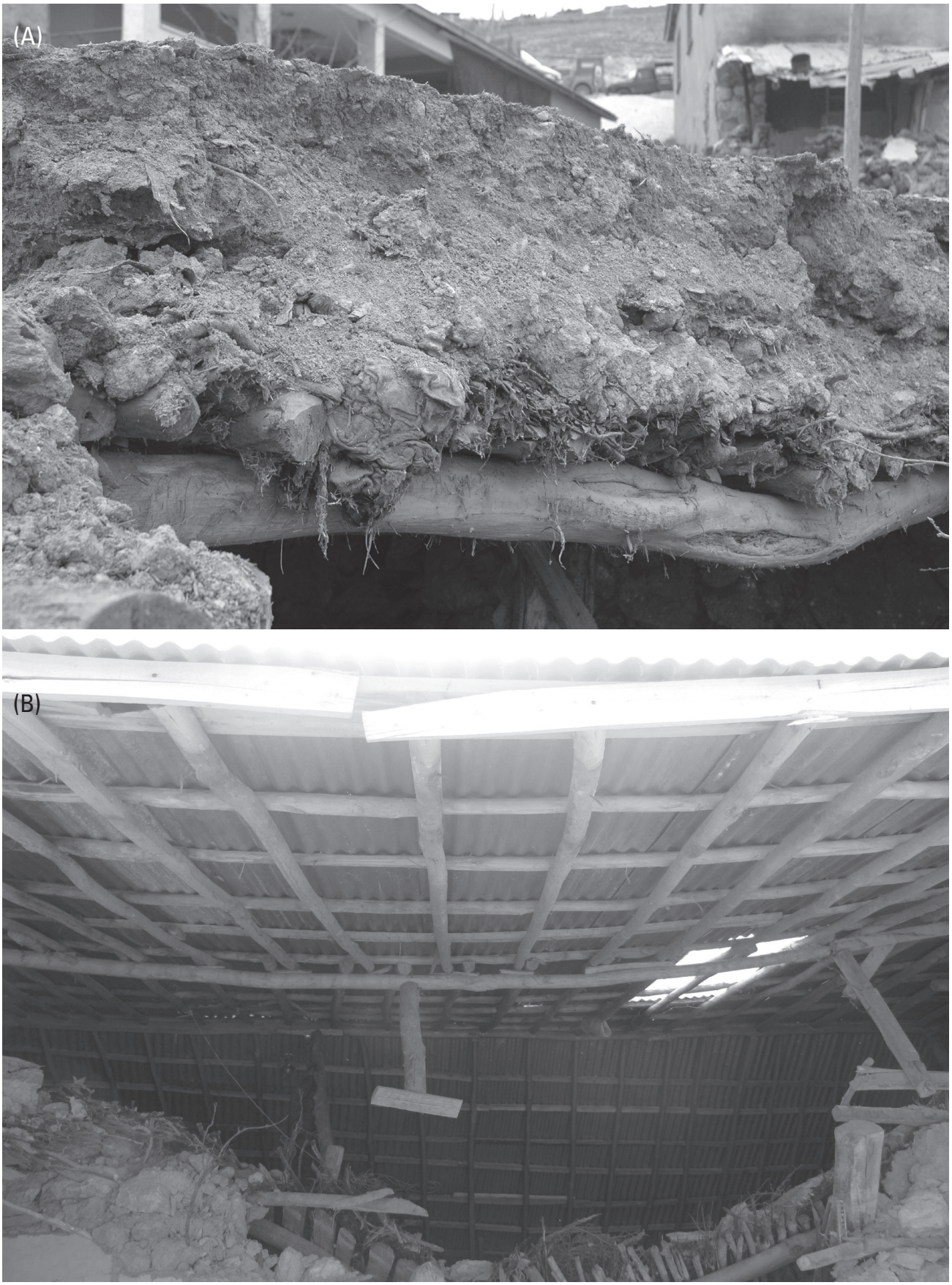

▲ **Figure 6.** A) Heavy earthen roofs. B) Light sheet-metal roof supported by wooden logs.

▲ **Figure 7.** Local buildings classified according to structural typology. Examples of A) Type I, B) Type II buildings (continued next page).

▲ **Figure 7 (continued).** Local buildings classified according to structural typology. Examples of C) Type III, and D) Type IV buildings.

▲ **Figure 8.** Out-of-plane failures of walls due to A) large unsupported wall length, B) poor wall-to-wall connection (continued next page).

▲ **Figure 8 (continued).** Out-of-plane failures of walls due to C) poor wall-to-floor connection, and D) unstable gable end wall.

(Figure 8B), and poor wall-to-wall connections (Figure 8C). In the absence of connecting units and proper detailing at the connections of perpendicular walls, the walls are separated from each other and behave like single walls that are weak in the out-of-plane direction. We also observed the collapse of gable end walls during the field investigations (Figure 8D).

For Type I and III buildings, in-plane failure modes were not frequently observed since the buildings are so poorly constructed and detailed that the walls generally collapsed in the out-of-plane direction. For Type II buildings, in the cases where out-of-plane failure was prevented, in-plane damage was observed in the form of horizontal cracks indicating sliding and rocking behavior and X-shaped cracks indicating diagonal shear mechanism.

Many Type I buildings collapsed due to the absence of structural integrity of vertical load-carrying members because wall-to-wall and wall-to-floor connections were not adequate. The early indications of this failure mode appear as damage at the corners of walls and at the top of the walls where they are supposed to be connected to the floor slab.

Reinforced Concrete Frame Buildings (Type IV)

With a few exceptions, the reinforced concrete buildings performed well during the earthquake. Most of them show light or no damage with hairline cracks or non-structural damages. Consequently, they could be occupied immediately after the earthquake.

School Buildings

Primary school buildings in the affected villages were stone masonry buildings of Type I and II, and they experienced significant damage during the earthquake. The school building in Yukarı Demirci collapsed. A closer look at the collapsed school building revealed that there was a ring beam at the roof level of the building that was supposed to be made of reinforced concrete, but it was "reinforced stone," *i.e.*, pieces of crushed stone inside a reinforcement cage with an inadequate amount of mortar to hold the pieces together and to fill the spaces (Figure 9). Primary school buildings in two other villages were also severely damaged. Hence, it was fortunate that the earthquake did not happen during daytime when the students would have been in their classrooms.

Mosques and Minarets

Mosques and minarets were also damaged in the villages during the earthquake. Figure 10A shows the interior view of the mosque in Yukarı Kanatlı village. It was a Type II stone masonry building with out-of-plane damage to its exterior walls. Minarets in three of the villages were also destroyed (Figure 10B).

QUANTIFICATION OF OBSERVED DAMAGE

Based on the field observations, it is possible to quantify the observed damage by type and class of building in the vicinity of the most affected villages. For quantification of damage, we employed the European Macroseismic Scale (EMS) (Grünthal 1998). The EMS scale provides damage grade charts separately for masonry and reinforced concrete structures. Damage grades range between 1 and 5, with the former representing negligible to slight damage and the latter representing total collapse or destruction.

According to the field observations, most of the buildings in Type I (Class A according to EMS) collapsed (Grade 5 according to EMS), most of the buildings in Type II (Class B according to EMS) suffered moderate damage (Grade 3 according to EMS), most of the buildings in Type III (Class A according to EMS) were heavily damaged (Grade 4 according to EMS), and most of the buildings in Type IV (Class C according to EMS) were slightly damaged (Grade 2 according to EMS). Comparing the observed damage with the definitions given in the EMS intensity scale, it is observed that EMS Intensity VIII (heavily damaging) can be assigned to the most heavily affected region (including the villages of Okçular, Yukarı Kanatlı, Tabanözü, and Yukarı Demirci) for the March 2010 earthquake.

A final comment on building practices is illustrated vividly in Figure 11, which shows damage to the type of rural buildings that have been described in this report. With little differences in the way dwellings are built (usually by their owners) between 1977 and 2010, there is also little difference in their seismic capacities. Minor improvement in details would have served to avoid collapses and the resulting losses of life.

CLOSING OBSERVATIONS

The Elazığ -Kovancılar earthquake of 8 March 2010 was not a major seismic event, but it confirmed the scientific benefit of Turkey's expanded national strong-motion network because it provided data for a moderate-magnitude event at moderate and long distances. The regional variation of recorded ground motions shows major differences from GMPEs of both domestic and global character.

The engineering reconnaissance showed that despite important advances toward achievement of seismic safety elsewhere in the country, rural areas with low economic status still lack adequate life safety. Of particular concern is the poor performance of school buildings, the most widely used facilities. An inspection program must be immediately undertaken for school buildings similar to those that were damaged beyond repair.

ACKNOWLEDGMENTS

The two EERC-METU teams that visited the stricken area within ten days of the event were the recipients of the hospitality and material support of Fırat University. We thank the rector of the university, Professor Fevzi Bingöl, and Professor Yusuf Calayır of the Department of Civil Engineering for having enabled transportation and logistical support. We also acknowledge the METU administration for the rapid deployment they enabled. Finally, we would like to thank Vladimir Graizer and Yahya Kurama for their reviews of this article.

▲ **Figure 9.** Collapsed stone masonry school building in Yukarı Demirci village. A) Exterior view. B) Closer look at the reinforced stone ring beam at the roof level.

▲ **Figure 10.** A) Interior view of the damaged mosque in Yukarı Kanatlı village. B) Damaged minaret in Yukarı Demirci village.

▲ **Figure 11.** Photos taken from collapsed rural masonry buildings. A) During the Elazığ Palu earthquake in 1977. B) Elazığ Kovancılar earthquake in 2010.

REFERENCES

Akkar, S., and Z. Cagnan (2010). A local ground motion predictive model for Turkey and its comparison with other regional and global ground-motion models. *Bulletin of the Seismological Society of America* **100** (6), 2,978–2,995.

Ambraseys, N. (2009). *Earthquakes in the Mediterranean and Middle East: A Multidisciplinary Study of Seismicity up to 1900*. Cambridge: Cambridge University Press.

Barka, A. (1996). Slip distribution along the north Anatolian fault associated with the large earthquakes of the period 1939 to 1967. *Bulletin of the Seismological Society of America* **86**, 1,238–1,254.

Boore, D. M., and G. M. Atkinson (2008). Ground motion prediction equations for the average horizontal component of PGA, PGV, and 5%-damped PSA at spectral periods between 0.01 s and 10.0 s. *Earthquake Spectra* **24** (1), 99–138.

Boore, D. M., W. B. Joyner, and T. E. Fumal (1997). Equations for estimating horizontal response spectra and peak acceleration from western North American earthquakes: Asummary of recent work. *Seismological Research Letters* **68**, 128–153.

Boore, D., C. D. Stephens, and W. B. Joyner (2002). Comments on baseline correction of digital strong motion data: Examples from the 1999 Hector Mine California earthquake. *Bulletin of the Seismological Society of America* **92** (4), 1,543–1,560.

Campbell, K. W., and Y. Bozorgnia (2008). NGA ground motion model for the geometric mean horizontal component of PGA, PGV, PGD and 5% damped linear elastic response spectra for periods ranging from 0.01 to 10 s. *Earthquake Spectra* **24** (1), 139–172.

Chiou, B., R. Darragh, N. Gregor, and W. J. Silva (2008). NGA project strong motion database. *Earthquake Spectra* **24** (1), 23–44.

Chiou, B. S.-J, and R. R. Youngs (2008). An NGA model for the average horizontal component of peak ground motion and response spectra. *Earthquake Spectra* **24** (1), 173–215.

Graizer V. (1989). Bearing on the problem of inertial seismometry. *Izvestya USSR Academy of Sciences, Physics of the Solid Earth* **25** (1), 26–29.

Graizer, V., and E. Kalkan (2007). Ground motion attenuation model for peak horizontal acceleration from shallow crustal earthquakes. *Earthquake Spectra* **23**, 585–613.

Graizer, V., and E. Kalkan (2009). Prediction of response spectral acceleration ordinates based on PGA attenuation. *Earthquake Spectra* **25** (1), 36–69.

Grünthal, G., ed. (1998). *European Macroseismic Scale 1998*. Cahiers du Centre Européen du Géodymamique et de Séismologie 15. Luxembourg: Centre Européen de Géodynamique et de Séismologie, 99 pps.

Kalkan, E., and P. Gülkan (2004). Site-dependent spectra derived from ground motion records in Turkey. *Earthquake Spectra* **20** (4), 1,111–1,138.

Kalkan, E., and S. K. Kunnath (2006). Effects of fling-step and forward directivity on the seismic response of buildings. *Earthquake Spectra* **22** (2), 367–390.

Lin, J., and R. S. Stein (2004). Stress triggering in thrust and subduction earthquakes, and stress interaction between the southern San Andreas and nearby thrust and strike-slip faults. *Journal of Geophysical Research* **109**, B02303; doi:10.1029/2003JB002607.

Sandıkkaya, M. A., M. T. Yılmaz, B. B. Bakır, and Ö. Yılmaz (2010). Site classification of Turkish national strong-motion stations. *Journal of Seismology* **14**, 543–563; doi: 10.1007/s10950-009-9182-y).

Saroglu, F., O. Emre, and I. Kuscu (1992). *Active Fault Map of Turkey*. General Directorate of Mineral Research and Exploration, Turkey.

Toda, S., R. S. Stein, K. Richards-Dinger, and S. Bozkurt (2005). Forecasting the evolution of seismicity in southern California: Animations built on earthquake stress transfer. *Journal of Geophysical Research* B05S16; doi:10.1029/2004JB003415.

Turkish Earthquake Code. (2007). *Specification for Structures to be Built in Disaster Areas*. TEC-07. Ankara, Turkey: Turkish Ministry of Public Works and Settlement.

Utkucu, M., S. S. Nalbant, J. McCloskey, S. Steacy, and Ö Alptekin (2003). Slip distribution and stress changes associated with the 1999 November 12 (Düzce) earthquake (*Mw* = 7.1). *Geophysical Journal International* **153**, 229–241.

Wells, D., and K. Coppersmith (1994). New empirical relationships among magnitude, rupture length, rupture width, rupture area, and surface displacement. *Bulletin of the Seismological Society of America* **84**, 974–1,002.

Zor, E., E. Sandvol, J. Xie, N. Türkelli, B. Mitchell, A. H. Gasanov, and G. Yetirmishli (2007). Crustal structure within the Turkish plateau and surrounding regions. *Bulletin of the Seismological Society of America* **97**, 151–161.

Earthquake Engineering Research Center
Middle East Technical University
06531 Ankara, Turkey
(A. A.)
aaskan@metu.edu.tr